Applied Catalysis B: Environment and Energy 353 (2024) 124095

Contents lists available at ScienceDirect

Applied Catalysis B: Environment and Energy

journal homepage: www.elsevier.com/locate/apcatb

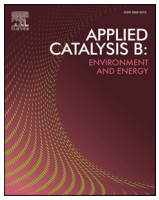

Efficient isomerization of glucose to fructose over Al-loaded functional lignin biopolymer

Jianrong Shan [a,1,2], Haixin Guo [a,1,3,*], Jiajiang Zhou [a,4], Feng Shen [a,5], Mo Qiu [a], Jirui Yang [a], Richard Lee Smith Jr [b,6,*], Xinhua Qi [c,7,*]

[a] Agro-Environmental Protection Institute, Ministry of Agriculture and Rural Affairs, No. 31 Fukang Road, Nankai, Tianjin 300191, China
[b] Graduate School of Environmental Studies, Tohoku University, Aramaki Aza Aoba 468-1, Aoba-ku, Sendai 980-8572, Japan
[c] College of Environmental Science and Engineering, Nankai University, No. 38, Tongyan Road, Jinnan, Tianjin 300350, China

ARTICLE INFO

Keywords:
Oxidative pretreatment
Hydrophilicity
Isomerization
Aluminum-doped
Lignin-based

ABSTRACT

Al-loaded functional lignin biopolymer (Al_x-Lbp) catalysts were synthesized using H_2O_2 oxidized alkali lignin and aluminum acetate via mechanochemical modification without post-calcination treatment. The Al_x-Lbp catalysts exhibited higher hydrophilicity and lower surface energy than lignin-free Al-activated carbon catalysts. Unprecedented high yields (58.5 %) of fructose from glucose were obtained over Al_1-Lbp in ethanol at 140 °C in 30 min reaction time. Al_1-Lbp catalyst had Lewis acid sites (47.2 μmol/g), Brønsted acid sites (6.9 μmol/g) and a surface energy of 39.1 mN/m that facilitated glucopyranose ring-opening and gave a glucose isomerization activation energy of 65.2 kJ/mol, which was lower than values reported for Lewis acid-catalyzed systems. Active sites of Al_2O_3 and $Al(OH)_3$ formed on the Al_1-Lbp catalyst in ethanol promoted the formation of an enediol intermediate as confirmed with isotope experiments to achieve efficient isomerization of glucose to fructose. The Al_1-Lbp catalyst demonstrated recyclability and maintained its initial activity for eight times reuse.

1. Introduction

Energy crises and increasing environmental pollution require development of sustainable and clean approaches that use renewable resources for chemical production [1,2]. Although feedstocks based on lignocellulosic biomass can create opportunities for sustainable chemical and food production, their conversion involves cascade reaction steps, including separation of lignin, hydrolysis of cellulose to glucose and further transformations [3,4]. Glucose isomerization is considered to be the key step for achieving conversion of lignocellulosic biomass into chemicals and food and it is the rate-limiting step [5]. Presently, isomerization of glucose to fructose is via fermentation (e.g., glucose isomerase) [6] or by chemical catalytic isomerization involving homogeneous and heterogeneous catalysis [7]. Biological conversion processes are widely used in the industrial production of fructose, but they have inherent drawbacks such as low efficiency, cost, and narrow scope of product applications [8] and furthermore, because they are equilibrium-limited (maximum 52 % glucose from fructose), either intensive separation steps or precise design of yeast strains are necessary to effectively produce other chemical products such as rare sugars [9].

Chemical catalytic isomerization has been suggested as a way to widen the scope of possible chemical products from glucose with

* Corresponding authors.
E-mail addresses: haixin_g@126.com (H. Guo), richard.smith.c6@tohoku.ac.jp (R.L. Smith Jr), qixinhua@nankai.edu.cn (X. Qi).
[1] Haixin Guo and Jianrong Shan contributed equally to this manuscript.
[2] **ORCID IDs:** https://orcid.org/0000-0001-8931-4265
[3] **ORCID IDs:** https://orcid.org/0000-0002-0864-5845
[4] **ORCID IDs:** https://orcid.org/0009-0005-9431-7045
[5] **ORCID IDs:** https://orcid.org/0000-0002-6292-0094
[6] **ORCID IDs:** https://orcid.org/0000-0002-9174-7681
[7] **ORCID IDs:** http://orcid.org/0000-0002-3227-7341

https://doi.org/10.1016/j.apcatb.2024.124095
Received 29 January 2024; Received in revised form 16 April 2024; Accepted 18 April 2024
Available online 19 April 2024

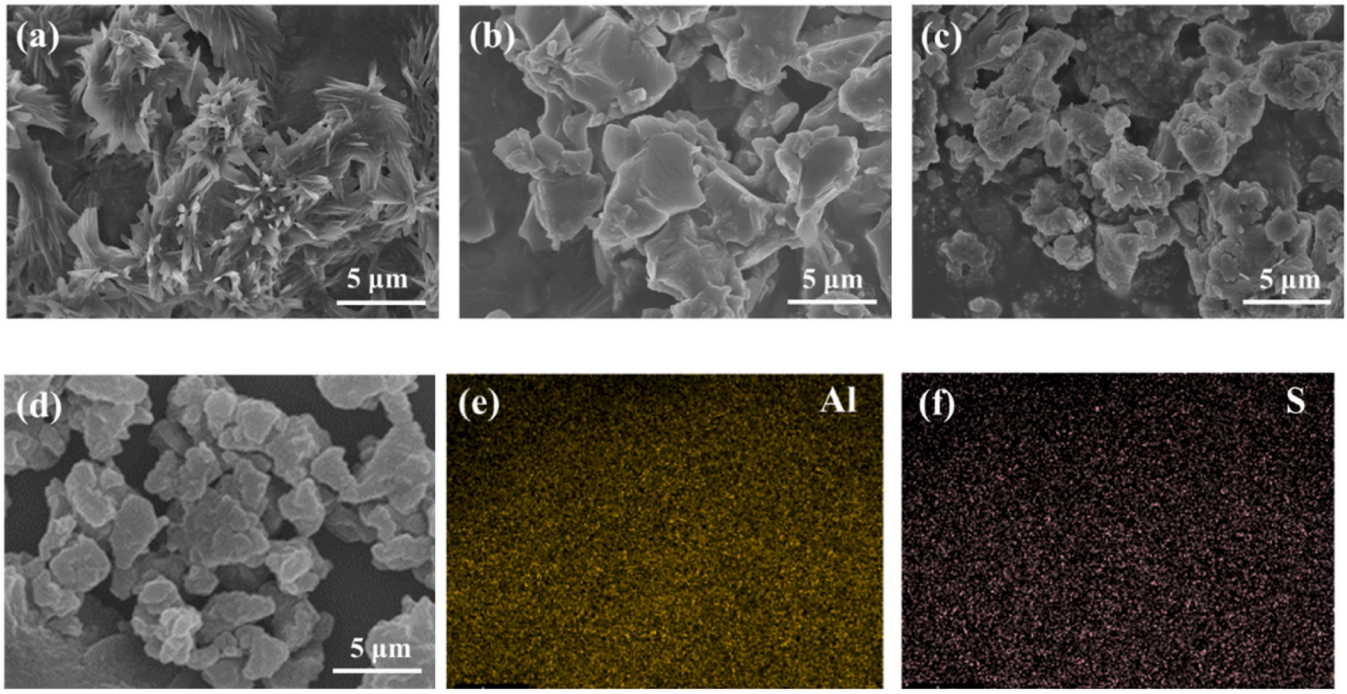

Fig. 1. Morphology and characterization of Al-loaded functional lignin biopolymer. SEM images: (a) Alkali lignin, (b) Lbp, (c) Al-Alkali lignin, (d) Al_1-Lbp. Mapping images: (e) Al, (f) S.

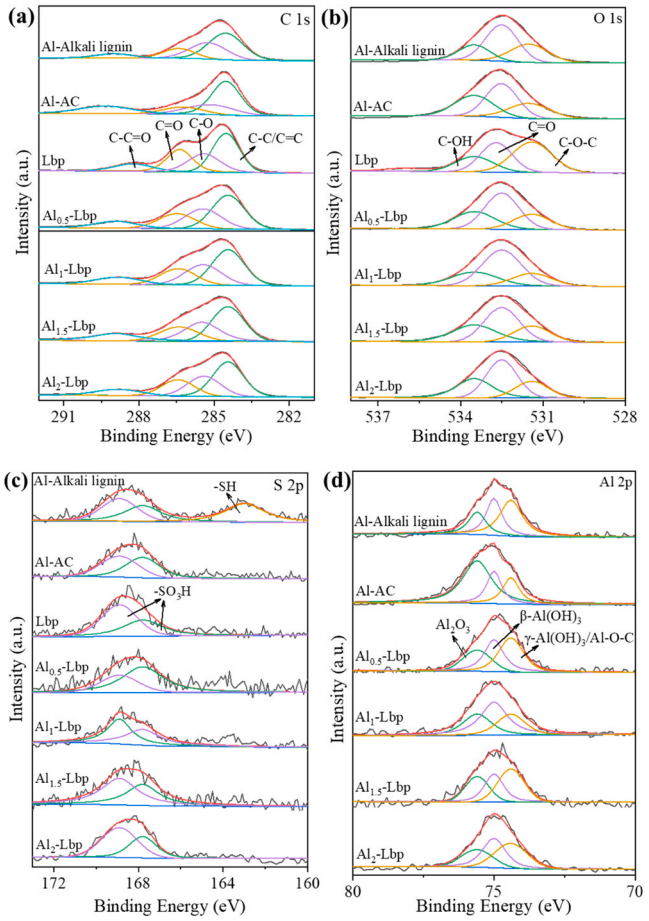

Fig. 2. X-ray photoelectron spectra (XPS): (a) C 1 s, (b) O 1 s, (c) S 2p and (d) Al 2p.

metallic element (e.g. Sn, Al, Zr halides) containing materials, metal-organic frameworks (MOFs), and zeolites being proposed as heterogeneous catalysts [10,11]. Stability and reusability of the catalyst should also be prioritized during the design phase for commercial viability [12]. Considering the applicable catalyst support types (e.g. zeolites, silica), biopolymers have merits due to their ease of synthesis and modification, available functional groups, and chemical stability [13]. Lignin, with its rich content of phenolic and aliphatic hydroxyl-containing groups, is highly-suitable for preparation of polymeric materials and functional carbons [14] and was chosen for modification as one point of novelty in this work. Lignin is a non-value-added by-product of the paper and pulp industry and has an annual output exceeding 70 million tons with only 2 % being used in commercial applications [15] indicating its under-utilized potential. Lignin-based biopolymer materials are becoming recognized for their multifunctional roles as catalytic materials and supports [16,17].

In this work, Al-loaded functional lignin biopolymer catalysts were prepared by oxidative pretreatment of lignin that was followed by mechanochemical modification without any type of post-treatment calcination. According to the proposed procedure, elimination of post-treatment calcination through oxidative pretreatment of lignin to form a catalytically-active biopolymer material is a key point of novelty of this research. The as-prepared Al-loaded functional lignin biopolymer materials were applied as catalysts for glucose isomerization. The performance of the prepared catalysts in this work exceed that of previously reported works and moreover, stability and reusability of the biopolymer catalysts are realized. Glucose isomerization mechanisms are elucidated by physical property measurements and in-situ FT-IR and ^{1}H NMR analyses.

2. Experimental

2.1. Materials

Lignin (Alkali lignin) and activated carbon (AC, 8–16 mesh) was purchased from Merck Sigma-Aldrich. D-glucose (≥99.5 %) and ethanol-OD (ethanol-d1) were supplied by Shanghai Aladdin Corp. Aluminum

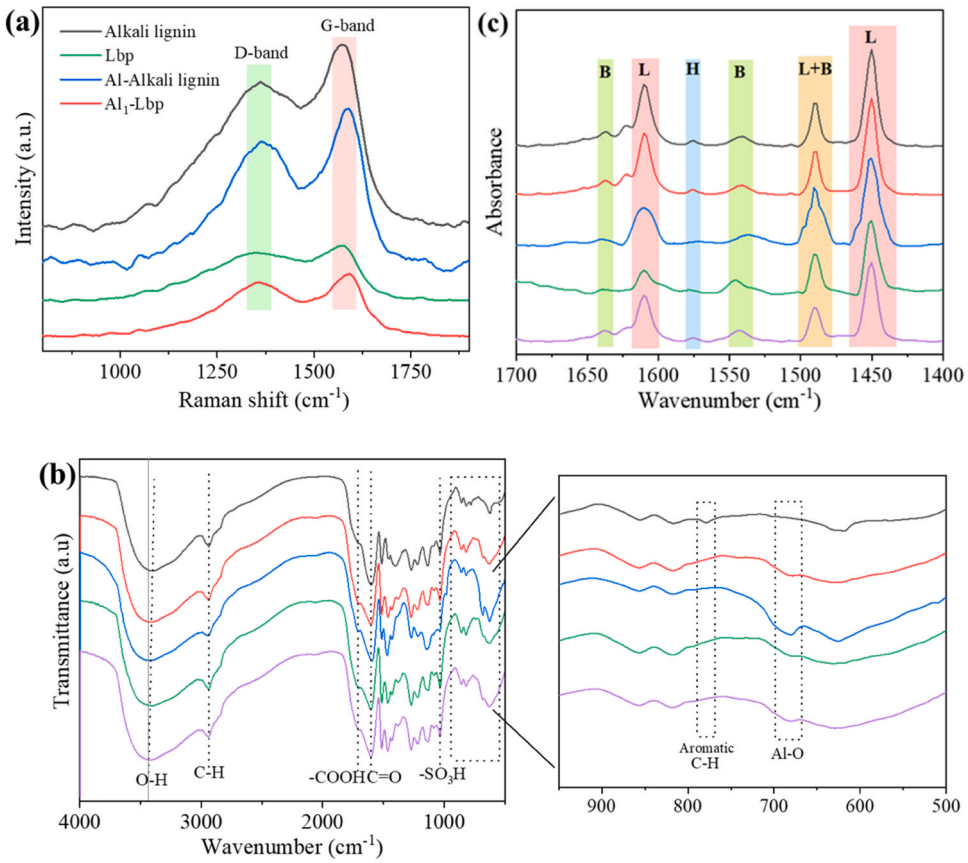

Fig. 3. Characterization of catalysts: (a) Raman spectra, (b) FTIR spectra (c) Py-FTIR spectra. Annotation. B: Brønsted acid site, L: Lewis acid site, H: H bound pyridine. Materials: (black line): Lbp; (red line): $Al_{0.5}$-Lbp; (blue line): Al_1-Lbp; (green line): $Al_{1.5}$-Lbp; (purple line): Al_2-Lbp.

Table 1
Summary of isomerization of glucose to fructose results and literature studies along with characterization of materials and catalysts: fresh lignin (Alkali lignin), oxidized-lignin (Lbp), ball-milled aluminum acetate with fresh lignin (Al-Alkali lignin) or with oxidized-lignin (Al_x-Lbp), activated carbon (AC) and Al-loaded AC*.

Entry	Catalyst	S_{BET}	Functional group content (mmol/g)		Acid content (μmol/g)		B/L ratio	Glucose conc.	*T*, time	Conv.	Yield	TOF	Ref.
		m^2/g	-COOH	-OH	B	L		g/L	(°C, min)	(%)	(%)	(min^{-1})	
1	-	-	-	-	-	-	-	36	140, 30	9.9±1	0	-	This work
2	Alkali lignin	2.6	2.5	0.5	3.6	30.4	0.12	36	140, 30	89.6±1	21.8±1	-	This work
3	Lbp	1.2	3.5	0.8	5.9	35.7	0.17	36	140, 30	51.5±1	25.2±1	-	This work
4	Al-Alkali lignin	3.0	2.1	0.6	-	-	-	36	140, 30	67.1±1	37.1±1	-	This work
5	$Al_{0.5}$-Lbp	7.6	3	1.5	9.0	41.1	0.22	36	140, 30	83.7±1	52.6±1	134.5	This work
6	Al_1-Lbp	9.9	2	1.8	6.9	47.2	0.15	36	140, 30	84.6±1	58.5±1	165.9	This work
7	$Al_{1.5}$-Lbp	4.8	4	0.8	13.4	36.4	0.37	36	140, 30	84.0±1	56.6±1	126.5	This work
8	Al_2-Lbp	5.5	3.5	0.3	9.2	30.9	0.3	36	140, 30	85.4±1	55.9±1	134.3	This work
9	AC	-	-	-	-	-	-	36	140, 30	6.4±1	-	-	This work
10	Al-AC	-	-	-	4.5	26.3	0.17	36	140, 30	29.5±1	12.1±1	-	This work
11	20 %Al-500 N_2	32.7	-	-	-	-	-	50	160, 20	29.2	21.5	14.2	[41]
12	Al-Cel-HTC220	68.1	-	-	-	-	-	50	160, 10	13.6	13.4	29.8	[33]
13	Al/HPHMs	-	-	-	-	-	-	40	160, 20	34.9	32.6	41.7	[42]
14	0.5Al–UCN	-	-	-	-	-	-	8.3	160, 180	71.7	48.3	21.5	[6]
15	Al/HC-300	78.5	-	-	-	-	-	50	160, 30	41.1	24.4	90.7	[25]
16	Mg-Al HT	-		-	-	-	-	100	120, 300	62.0	51.0	-	[43]

* HPHMs: hierarchically porous structure; UCN: Graphitic carbon nitride; HT: Hydrotalcite; TOF: turnover frequency (TOF) = (moles of fructose)/(moles of Al revealed by SEM-EDX × 10^{-3} × time) [44].

acetate ($C_6H_9AlO_6$) and D-fructose (99 %) were bought from Macklin Regent company. The solvent ethanol (99.5 %) and 30 % H_2O_2 was supplied by Tianjin Fengchuan Chemical Reagent Co. Ltd. All chemicals were used as received without further purification or pretreatment steps.

2.2. Synthesis of lignin-derived carbon

Generally, 5.0 g lignin was pretreated with 12.5 mL of H_2O_2 solution at room temperature for 18 h, and then washed with water and dried at 80 °C for 12 h. The obtained solids were denoted as oxidized lignin

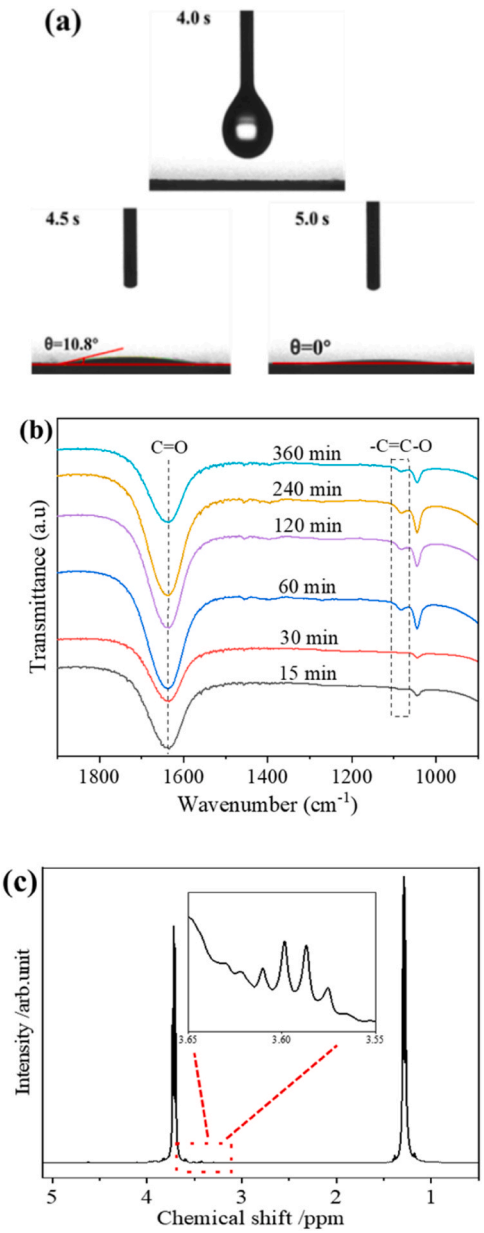

Fig. 4. Properties and reaction results with Al_1-Lbp catalyst for isomerization of glucose to fructose: (a) static contact angle with water or ethanol, (b) *In situ* FTIR spectra recorded during time-course of reaction (Reaction conditions: 180 mg glucose, 90 mg catalyst, 5 mL ethanol, 140 °C). (c) ^{1}H NMR spectra of solution after completion of reaction (Reaction conditions: 180 mg glucose, 90 mg catalyst, 5 mL ethanol-OD (ethanol-d1), 140 °C, 30 min reaction time).

Table 2
Contact angle and surface energy of as-prepared materials.

Material	Contact angle		Surface free energy
	Water	Ethanol	mN/m
Al_1-Lbp	71.4°	10.8°	39.1
Al-AC	29.4°	12.9°	153.2

biopolymer (Lbp). Then, 1.0 g Lbp and $x \times 10^{-2}$ moles of aluminum acetate were ball milled for 4 h, washed three times with deionized water, and dried at 80 °C. The obtained aluminum-containing solids were denoted as Al_x-Lbp. For comparison, Al-Alkali lignin prepared with non-oxidized lignin and Al-AC prepared with activated carbon (AC) instead of lignin were prepared as experimental blanks using the method described for Al_x-Lbp.

2.3. Characterization

Sample morphology was characterized by scanning electron microscopy (SEM, Regulus8100, Japan). XRD patterns of the materials were taken with a Bruker D8 Advance instrument using Cu-Kα radiation and a curved crystal graphite monochromator operated at 40 kV and 40 mA (λ=0.15405 nm). XPS measurements were carried out on an ESCALAB 250Xi (Thermo Fisher Scientific) instrument with monochrome Al-Kα (hv=1486.6 eV, power 150 W) radiation and binding energy was calibrated at C1s 284.8 eV. For determination of Lewis acid and Brønsted acid sites of the as-prepared materials, a Fourier transform infrared spectrometer (Bruker Tensor 27, Germany) was used to scan the pyridine vapor (Py-FTIR) in the range of (1400–1700) cm^{-1}. Infrared spectra of pyridine adsorption on the prepared catalysts at (50, 140, 300) °C were recorded and the content of Lewis acid and Brønsted acid sites were calculated as described in Supplementary Materials (Section A) using integrated molar extinction coefficients reported by Emeis [18]. The surface hydrophilicity and hydrophobicity of the catalysts were measured using a contact angle instrument (Dataphysics OCA20, Germany). Surface hydrophilicity was tested using 3 μL droplets of water or ethanol at room temperature, and surface hydrophobicity was determined by measuring contact angle between the droplet and the catalyst surface. Content of Al in the materials was measured by inductively coupled plasma-optical emission spectroscopy (ICP-OES) (Agilent 730, USA). Fourier transform infrared (FT-IR) spectra were recorded with a Nicolet iS5 spectrometer (Thermo Nicolet 8700). The Brunauer-Emmett-Teller (BET) using an automatic nitrogen adsorption analyzer (U.S. Merck ASAP2460) to obtain surface area and porosity characteristics.

2.4. Reaction experiments

Isomerization of fructose to glucose was carried out in a closed 10 mL microwave reactor under magnetic stirring. In a typical procedure, 0.18 g D-glucose, 0.09 mg catalyst, and 5 mL ethanol were added into the reactor. Then, the reactor was heated to the desired temperature of (100−160) °C with continuous stirring (600 rpm). After a given time, the reaction mixture was separated through a 0.22 μm syringe filter membrane and the filtrate solution was analyzed by ultra-high-performance liquid chromatography (Waters Acquity UPLC H-Class) equipped with a SHODEX SH1011 column and a refractive index (RI) detector. The mobile phase of the UPLC consisted of a 5 mmol/L sulfuric acid aqueous solution in which a 0.5 mL/min flow rate was used. Glucose conversion, fructose yield and fructose selectivity were calculated according to Eqs. (1)-(3):

$$\text{Glucose conversion } (\%) = \frac{\text{moles of reacted glucose}}{\text{initial moles of glucose loaded}} \times 100\% \quad (1)$$

$$\text{Fructose yield } (\%) = \frac{\text{moles of fructose in product}}{\text{initial moles of glucose loaded}} \times 100\% \quad (2)$$

$$\text{Selectivity } (\%) = \frac{\text{moles of fructose}}{\text{initial moles of glucose loaded} - \text{final moles of glucose remaining}} \times 100\% \quad (3)$$

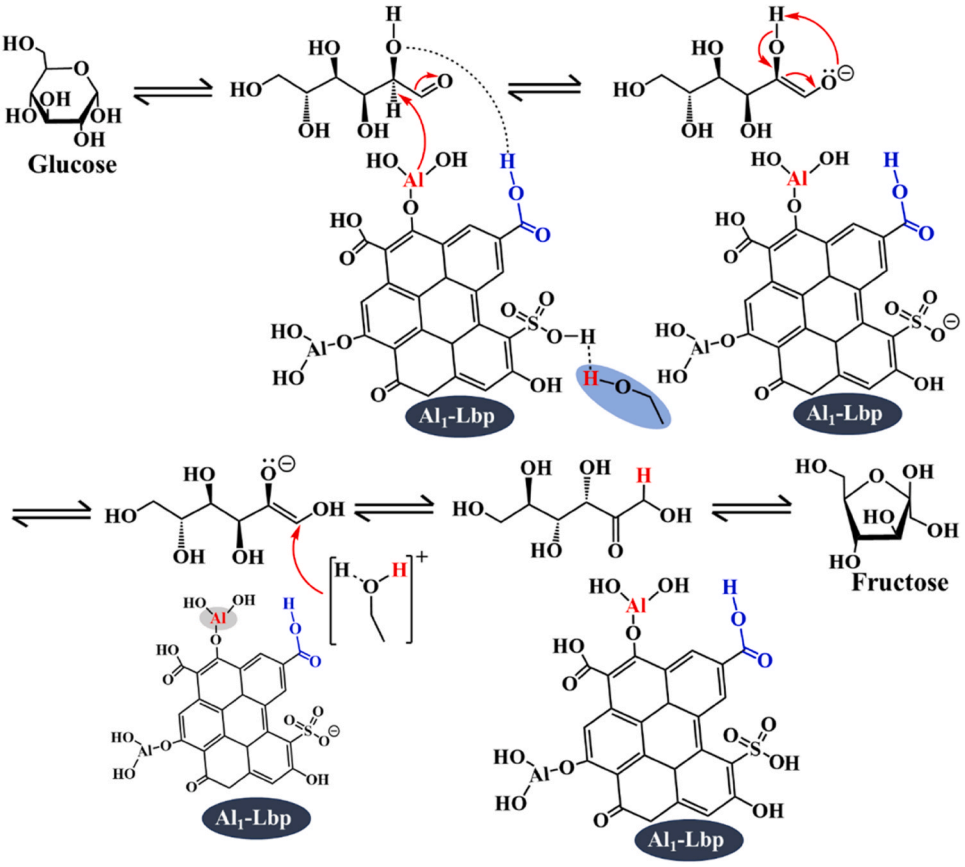

Scheme 1. Schematic representation of glucose isomerization mechanism over Al_1-Lbp catalyst in ethanol.

Table 3
Effect of reaction temperature on isomerization of glucose over Al_1-Lbp catalyst. (Reaction conditions: 0.18 g glucose, 0.09 g catalyst. 5 mL ethanol).

Entry	*T*	Time	Conv.	Fructose yield	Selectivity
	(°C)	(min)	(%)	(%)	(%)
1	100	60	23.9	9.4	39.3
2		90	29.1	14.9	51.2
3		120	32.5	19.0	58.5
4		240	42.8	29.3	68.5
5		360	55.6	33.0	59.4
6		480	90.3	49.4	54.7
7	120	15	33.5	19.9	59.4
8		30	43.7	27.1	62.0
9		60	59.4	40.5	68.2
10		90	70.5	46.3	65.7
11		120	74.8	52.5	70.2
12		240	88.6	54.8	61.9
13		360	91.0	52.4	57.6
14	140	10	66.7	41.6	62.4
15		15	72.7	48.5	66.7
16		30	84.6	58.5	69.1
17		60	90.9	56.7	62.4
18		90	93.2	51.9	55.7
19		120	93.8	38.1	40.6
20		240	93.8	28.3	30.2
21	160	5	84.5	52.4	62.0
22		10	90.7	53.7	59.2
23		15	92.8	50.9	54.8
23		30	94.8	31.3	33.0

All results were replicated at least three times, and the reproducibility of fructose yields were within 3 % standard deviation.

2.5. Kinetic experiments

Kinetic experiments of glucose isomerization were performed in the temperature range of (120−160) °C under optimized reaction conditions. The following assumptions were used in the analyses:

(1) Main reaction was glucose to fructose; all side-reactions were neglected;
(2) Main reaction was irreversible and occurred by pseudo first-order kinetics;
(3) All by-products were considered to be degradation compounds (humins);
(4) All by-products had negligibly low concentrations.

With the above assumptions, rate constants at different temperatures were calculated according to the following Weibull equation [18]:

$$-ln\left(\frac{C_t}{C_0}\right) = kt \tag{3}$$

where k, t, C_0 and C_t represent the reaction rate constant (min^{-1}), reaction time (min), glucose concentration (mol/mL) at 0 min and at time t, respectively. The activation energy of glucose isomerization was estimated using the Arrhenius equation [19]:

$$lnk = -\frac{E_a}{RT} + \ln A \tag{4}$$

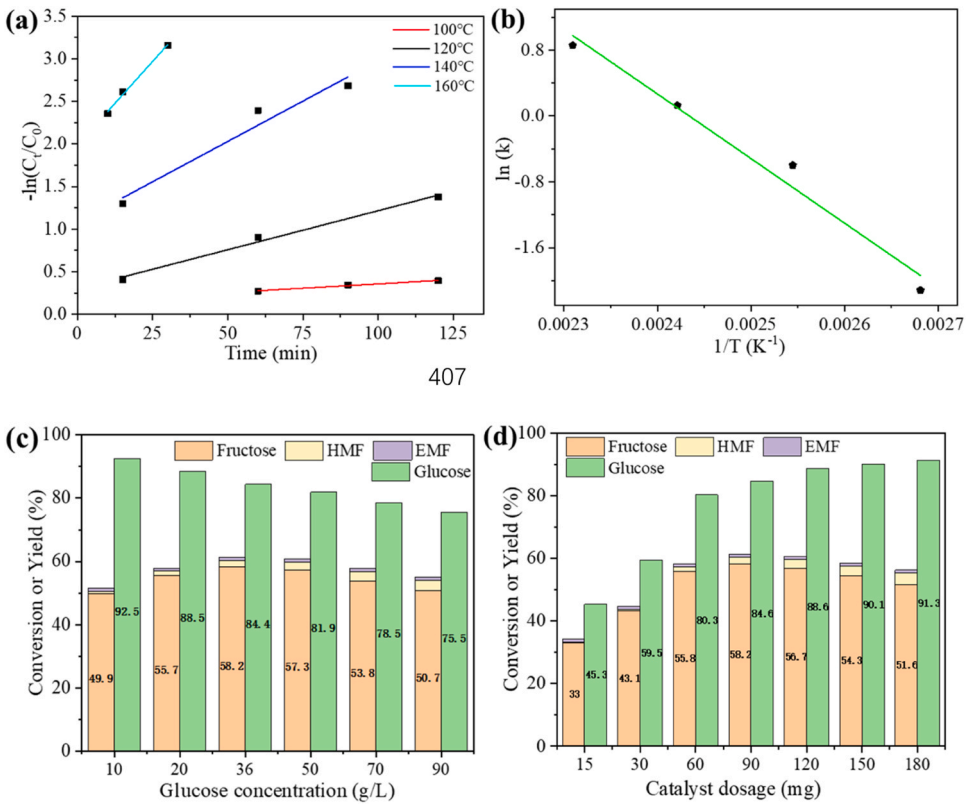

Fig. 5. Reaction kinetics for isomerization of glucose to fructose over Al_1-Lbp catalyst in ethanol solvent: (a) kinetic analysis, (b) Arrhenius plot of glucose isomerization catalyzed by Al_1-Lbp in ethanol, (c) influence of initial substrate concentrations, (d) influence of catalyst dosage. Conditions unless specified otherwise: 90 mg catalyst dosage, 5 mL ethanol, 140 ℃ reaction temperature, 30 min reaction time.

Table 4
Kinetic parameters for isomerization of glucose to fructose in ethanol over Al_1-Lbp catalyst.

T (℃)	Kinetic analysis		Arrhenius plot	
	Rate constant, *k* (min^{-1})	R^2	Activation energy, E_a (kJ/mol)	R^2
100	0.1206	0.9898	65.2	0.9755
120	0.5495	0.9913		
140	1.1369	0.9570		
160	2.3570	0.9947		

where E_a, *T*, *R* and *A* represent the activation energy (kJ/mol), reaction temperature (K), gas constant (0.008314 kJ mol^{-1} K^{-1}), and pre-exponential factor (min^{-1}), respectively.

FTIR spectra was used to monitor the solution continually during microwave reaction for the mechanistic study. Briefly, at the same temperature and at different reaction times, 0.05 mL of solution after microwave reaction was taken, diluted 10 times and placed between potassium bromide (KBr) plates (25*4 mm) and placed in an FTIR instrument. Variation of FTIR spectra with reaction time was compiled to understand the time course of the species being consumed and formed.

3. Results and discussion

3.1. Characterization of materials and catalysts

SEM images showed that the fresh alkali lignin was composed of irregular spiny-like structures (Fig. 1a). After the lignin was oxidized, the resulting Lbp material had relatively smooth block-like particles (Fig. 1b). When the materials were doped with metal Al ions, Al-Alkali lignin and Al-Lbp formed rough and bonded-block particles (Figs. 1c-1d), which can be attributed to structural branches and protrusions during oxidation being destroyed or melded with the surface [20]. The roughness of the particles may also cause formation of active sites on the surface of the crystal plane loaded with Al, making the arrangement of these sites lead to the formation of coarse structures on the particle surfaces [21]. Al and S elements were uniformly distributed on the catalyst surface and had a relative atomic content of 2.2 % for Al loading and 0.6 % for S loading (Fig. 1e-f and Fig. S1).

XPS analyses (Fig. 2) confirmed the existence of C, O, S, and Al elements in the as-prepared catalyst. Characteristics peaks for C 1 s at (284.7, 285.5, 286.5, 288.7) eV corresponding to (C-C/C═C, C-O, C═O, C-C═O), respectively were observed (Fig. 2a) [22]. The O 1 s spectrum could be deconvoluted into three types of oxygen at (531.5, 532.5, 533.5) eV corresponding to (C-O-C, O-C, C-OH) bonds, respectively (Fig. 2b) [23]. Compared with Lbp, the peak area of functional group C-O-C decreased from 42.4 % to about 20 % after Al was loaded, suggesting the cleavage of ether bonds and formation of complexes. For S 2p spectra, peaks at (167.8,168.9) eV correspond to the 2p 3/2 and 1/2 orbits of the -SO_3H group, respectively (Fig. 2c), suggesting that -SH groups of alkali lignin had been oxidized into -SO_3H groups by H_2O_2 [24]. For Al 2p spectra, signals located at (75.6, 75, 74.4) eV refer to Al_2O_3, β-$Al(OH)_3$, Al-O-C or γ-$Al(OH)_3$, respectively [25]. The Al 2p peak at 74.4 eV is attributed to the C-O-Al group (Fig. 2d), and illustrates that Al metal binds to hydrocarbons through a metal-oxo-carbon bridge [26], which is possibly due to Lbp having a large number of oxygen-containing functional groups that tend to form Al^{3+} species such as $Al(OH)_3$ and Al_2O_3 structures during the ball-milling treatment process [27]. XPS analyses of the Al-loaded functional lignin biopolymer showed its major surface element was carbon, which should make the material hydrophilic, whereas considerable amounts of oxygen-containing functional groups most likely further enhanced the

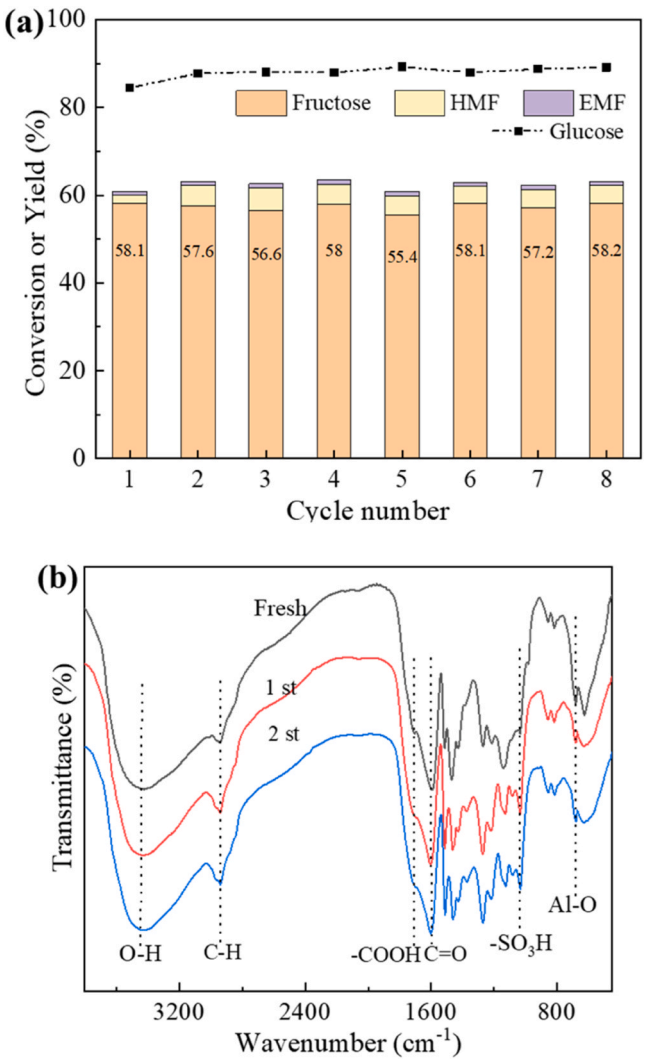

Fig. 6. Recycling of Al_1-Lbp catalyst in isomerization of glucose to fructose: (a) catalytic activity and (b) FTIR spectra of fresh and used Al_1-Lbp. (Reaction conditions: 180 mg glucose, 90 mg catalyst, 5 mL ethanol, 140 °C, 30 min reaction time).

surface hydrophilicity. The content of different forms of aluminum on the surface of the materials was different. Al-AC had lower content of Al $(OH)_3$ groups than the Al-loaded functional lignin biopolymer. The Al_1-Lbp had the highest percentage of β-Al$(OH)_3$ groups among the Al-loaded functional lignin biopolymer (Table S2).

XRD patterns of Al-loaded functional lignin biopolymer (Fig. S3) exhibited peaks at 23.6° and 31.6° attributed to (002) and (220) planes of graphite, respectively [28]. No peaks were observed that could be attributed to Al metal, which may be due to Al metal being evenly distributed on the surface of the carbon material without crystalline metal or enriched areas [29].

Raman spectra of the catalysts (Fig. 3a) showed characteristic peaks at 1360 cm^{-1} (D-band) and 1588 cm^{-1} (G-band), which correspond to disordered and graphitic carbon structures, respectively [19]. Intensity ratios of the D-band to G-band (I_D/I_G) for Alkali lignin, Lbp, Al-Alkali lignin, and Al_1-Lbp were 2.4, 3.7, 1.6, and 2.2, respectively (Table S3), which suggests that the degree of graphitization increased after chemical pretreatment and mechanochemistry modification [30].

FTIR spectra of the catalysts had bands at 3420 cm^{-1}, 1710 cm^{-1}, 1620 cm^{-1} and 2925 cm^{-1} corresponding to the stretching mode of O-H, -COOH, C=O, and C-H in aromatic carbons respectively (Fig. 3b) [19, 24,31]. With increased Al loading (Fig. 3b), the interaction with the O-H (3420 cm^{-1}) bond in the catalyst lead to a shift of the peak position, while the signal intensities of C-H (2925 cm^{-1}) and C=O (1620 cm^{-1}) in the catalysts weakened and disappeared, which is possibly due to the aliphatic C-H stretching vibration and aromatic C-H (771.3 cm^{-1}) out-of-plane bending vibration [32,33]. When 1 $*10^{-2}$ mol aluminum acetate (Al_1-Lbp) sample material was measured (Fig. 3c), the peak intensity at 1620 cm^{-1} became the strongest and the hydrogen bond peak intensity at 1575 cm^{-1} became the lowest among the samples, implying that the introduced metal Al replaced the hydroxyl group on the original skeleton and weakened the strength of the B acid site, which is consistent with the results of Fig. 3b. The peak O-Al at 680 cm^{-1} related to tensile vibration appeared, which is attributed to grafting of Al metal onto oxygenated groups [34], suggesting that the functional groups on Lbp partially interacted or were replaced by Al metal ions and formed C-O-Al groups. The peak at 1033 cm^{-1} was attributed to the -SO_3H [24] and was consistent with the XPS (Al 2p) analysis results.

Py-FTIR analysis was performed to distinguish the types of acid sites on the catalysts (Fig. 3c). Peaks at 1446 cm^{-1} and 1620 cm^{-1} correspond to Lewis acid sites (L acid), and peaks at 1640 cm^{-1} and 1548 cm^{-1} correspond to Brønsted acid sites (B acid) [35]. Binding at 1490 cm^{-1} is attributed to L acid and B acid sites (L+B) [36]. When 1 $*10^{-2}$ mol aluminum acetate (Al_1-Lbp) was added, the peak intensity at 1620 cm^{-1} became the strongest and the hydrogen bond peak intensity at 1575 cm^{-1} became the lowest among the samples, implying that the introduced metal Al replaced the hydroxyl groups on the original skeleton and weakened the strength of the B acid site, which is consistent with the results of Fig. 3b.

Brønsted acid and Lewis acid site content of the catalysts was determined by Py-FTIR at 140 °C (Table 1), which shows that fresh lignin after H_2O_2 treatment (Lbp) was rich in -COOH and -OH functional groups, making these materials favorable for chemical adsorption [37]. Total acid amount (sum of L and B values) of lignin materials increased from 34.0 μmol/g (Alkali lignin) to 41.6 μmol/g (Lbp). For added Al content (Entries 5–8, Table 1), the Lewis acid content and the total acid amount increased first and then decreased. The Al_1-Lbp material had the highest Lewis acidity (47.2 μmol/g) and total acidity (54.1 μmol/g) among the materials. Total acidity (30.8 μmol/g) of activated carbon loaded with Al (Al-AC) was far lower than that of the Al_1-Lbp material (Table 1). Surface functional groups of alkali lignin increased after oxidation and seemed to synergistically interact with the loaded aluminum possibly because of interactions of surface functional groups adsorbing aluminum that enhanced formation of L acid sites in the synthesized materials. The density of -OH functional group increased from 0.8 mmol/g for Lbp to 1.8 mmol/g for Al_1-Lbp but decreased to 0.3 mmol/g for Al_2-Lbp (Table 1). While the density of -COOH functional groups decreased from 3.5 mmol/g for Lbp to 2 mmol/g for Al_1-Lbp, it increased to 4 mmol/g for $Al_{1.5}$-Lbp.

3.2. Catalytic investigation

Performance of catalysts applied to promote isomerization of glucose is summarized in Table 1. Isomerization of glucose did not occur in the absence of catalyst, while under high-temperature conditions, glucose and ethanol may undergo decomposition, oxidation or other side reactions [38], which probably resulted in conversion of glucose without catalyst (Entry 1, Table 1). When experiments were performed with lignin or oxidized lignin as catalysts (Entries 2–3, Table 1), fructose yields were less than 27 %. When Al-loaded lignin-based catalysts were used, fructose yields increased to as high as 58.5 % with conversions being higher than 80 % for the case when oxidized lignin was used (Entries 5–8, Table 1), suggesting that Lewis acidity of the Al site in the catalyst facilitated glucose isomerization. On the other hand, when experiments were performed with AC (Entry 9, Table 1), isomerization did not proceed, while when Al-AC was employed (Entry 10, Table 1), fructose yields were less than 13 %, inferring that although Al has Lewis acidity, functionalization of lignin is important for promoting the

reaction and furthermore, it is possible that glucose isomerization kinetics are related to $Al(OH)_3$ groups rather than to Al_2O_3 groups [26]. With an increase in Al loading in the oxidized-lignin samples (Entries 5–8, Table 1), turnover frequency (TOF; moles of fructose per mole of Al revealed by SEM-EDX $\times 10^{-3}$) had a range of (126−166) min^{-1}, which were much higher than values reported for Al-containing heterogeneous catalysts in the literature (Entries 11–16, Table 1 and Table S4) [3,19]. The above results show that the Al-loaded functional lignin biopolymer materials were effective as catalysts for promoting the isomerization of glucose to fructose.

Static contact angle experiments were conducted to determine the surface wettability of the as-prepared catalysts in ethanol and water. Ethanol or water droplets at the surface of the Al_1-Lbp catalyst spread out immediately and the resulting contact angle was 10.8° for ethanol (Figs. 4a) or 71.4° for water indicating superhydrophilicity for polar solvents and possible lowering of the surface tension and surface energy of the catalytic surface. Surface energies of the as-prepared catalyst Al_1-Lbp (39.1 mN/m) and Al-AC (153.2 mN/m) were determined by the Owens-Wendt-Fowkes method (Table 2) [39]. A lower surface energy suggests that the catalyst surface has better wettability for polar substrates than less polar substrates, which can lead to reduced interaction between the catalyst and reaction substrate, while a high surface energy suggests factors such as metal agglomeration and reduced catalytic activity [40]. BET surface areas of all as-prepared lignin-based materials were small (< 10 m^2/g) (Entries 2–8, Table 1). On the other hand, the adsorption efficiency of glucose on Al-loaded functional lignin biopolymer was remarkable in that it had comparable adsorption capacity and characteristics as that of activated carbon (about 96 %) at room temperature and contact time of 30 min, which can be attributed to the amount oxygen-containing functional groups on the lignin-based materials (Section B, Supplementary Materials, Fig. S5). The as-prepared catalyst with its superhydrophilicity and high adsorption affinity for polar substrates, most likely lowered diffusional resistance of substrates to the catalyst active sites and facilitated glucose isomerization.

3.3. Reaction mechanism

FTIR spectra measurements were made of diluted solutions as the reaction progressed over the Al_1-Lbp catalyst (Fig. 4b). As shown in Table S5, yields of other product (HMF and EMF) were lower than 3 %. The peak at 1620 cm^{-1} in the infrared spectrum was assigned to the C═O vibration of glucose, which occurs in ring-opening [45]. Due to the low yield of by-products HMF and EMF, the appearance of the C-O peak at 1100 cm^{-1} indicates the formation of enolate intermediates through a tautomerism process [8,46].

The ^1H NMR analyses were performed on reaction solutions with ethanol-d1 as the reaction solvent (Fig. 4c). NMR spectrum (Fig. 4c) showed signals at 3.58–3.70 ppm corresponding to the D atom in the C1 of fructose [47], which suggests that H atoms in the C1 of fructose originated from the OH group of ethanol.

Based on above experimental results, a possible reaction mechanism for glucose isomerization with Al-loaded functional lignin biopolymer can be proposed (Scheme 1). Firstly, glucose is adsorbed on the catalyst surface and interacts with electron-rich functional groups. The -COOH groups on the catalyst dissociate in the presence of ethanol leading to the formation of a hydroxylated surface [48]. The $-SO_3H$ protonates ethanol to make it positively charged. Then, the cyclic structure of glucose opens in the presence of a Lewis acid site. The H atom at the C2 position in glucose is broken by the active center of the catalyst, forming an enediol intermediate, while H^+ is captured by negatively charged $-SO_3^-$. Through electron transfer and rearrangement, the enediol intermediate captures an H atom from ethanol, which results in fructose formation (Scheme 1). In summary, the Lewis acids and oxygen-containing groups on the Al_1-Lbp catalyst are pivotal in creating active sites, influencing the electronic structure, and promoting key steps in the isomerization of glucose.

3.4. Effect of reaction conditions on catalytic performance

The influence of reaction temperature, catalyst dosage and substrate concentration on the isomerization of glucose to fructose by the catalyst was investigated (Table 3). At a reaction temperature of 100 °C, the selectivity of fructose was 68.5 % at 240 min reaction time (Entry 4, Table 3). The highest selectivity and highest yield obtained for the reaction conditions studied were 70.2 % (Entry 11, Tables 3) and 58.5 % (Entry 16, Table 3), respectively. Acetalization products of fructose decreased with increasing reaction temperature and prolonged reaction time.

Rate constants of glucose isomerization at different temperatures were calculated according to the Weibull model [49]. Reaction rate constants increased with increasing reaction temperature and roughly doubled for every 20 °C increase in reaction temperature (Fig. 5a). Activation energy of glucose isomerization catalyzed by Al_1-Lbp was estimated to be 65.2 kJ/mol (Fig. 5b; Table 4) and was comparable with that of most heterogeneous Lewis acid-catalyzed systems such as Al-bentonite (59.0 kJ/mol) [50], $AlCl_3$ (59.0 kJ/mol) [51], Al/HC180–300/O (110.4 kJ/mol) [52] and other catalysts (54–108 kJ/mol) [53–55].

Influence of initial substrate concentration on the fructose yield by Al_1-Lbp catalyst was studied (Fig. 5c). At an initial glucose concentration of 36 g/L, the maximum fructose yield was obtained, but also formation of HMF and EMF were observed and higher initial concentrations of glucose led to higher yields of HMF and EMF while fructose yields declined (Fig. 5c). Glucose conversion slightly decreased to 84.4 % with a 58.2 % fructose yield (Fig. 5c), which suggests that the Al_1-Lbp based catalytic system is tolerant to high initial concentrations of glucose making it a candidate for large-scale systems. With an increase in glucose substrate concentration over 36 g/L, reaction rate increased and HMF and EMF production increased. Carbon balances were made for reactions studied at 140 °C for 30 min of reaction time over the full range of glucose concentrations (Fig. 5c) and are given in Supplementary Materials (Table S6); carbon balances were generally greater than 85 %. The remaining carbon species are most likely ethyl glucoside, since this compound forms as an intermediate from glucose and ethanol in the presence of a Brønsted acid site under low initial glucose concentration (e.g. 10 g/L). The ethyl glucoside will further undergo dehydration to 5-EMF and 5-EMF subsequently dehydration and ethanolysis to ethyl formate and ethyl levulinate under Bronsted acid conditions (Scheme S1) [56–58].

Influence of catalyst dosage on fructose yield (Fig. 5d) showed that a catalyst dosage of 90 mg in 5 mL ethanol gave a maximum in fructose yield. Further increasing catalyst amounts to 180 mg afforded 91.3 % glucose conversions and lower fructose yields (51.6 %), which may be related to the number of active sites in the catalytic reaction system. With an increase in catalyst dosage, the active sites of Al increase and dehydration reactions occur after glucose undergoes isomerization to produce HMF and other derivatives. As the reaction continues, derivatives gradually react, thereby increasing the glucose conversion.

3.5. Recycle and reuse

To study the stability and reusability of the as-prepared Al-loaded lignin-derived carbon, eight consecutive reaction cycles were performed (Fig. 6a). After each run, the catalyst was separated, washed with water and dried for the next run. Glucose conversion slightly increased over the recycling trials that can be attributed to adsorption and non-reaction of glucose on the catalyst, while HMF yields remained constant at about 4 % after the first reuse. The Al content in the fresh and spent catalysts was detected by ICP-OES, and was confirmed to change slightly (< 0.5 % for each run). Reused catalyst examined with FT-IR spectroscopy (Fig. 6b) confirmed that functional groups in the catalyst remained the same. From these results (Fig. 6), the catalyst could be confirmed to maintain its structure under reaction conditions and therefore, it can be

concluded that the catalyst was stable and durable.

4. Conclusions

In this work, a method was proposed to prepare Al-loaded functional lignin biopolymer through the use of oxidized lignin substrate by mechanochemistry. The catalysts were applied to glucose isomerization and were found to be efficient and selective with a 58.5 % fructose yield being obtained over Al_1-Lbp in ethanol solvent at a reaction temperature of 140 °C and 30 min reaction time. The favorable results for the Al-loaded functional lignin biopolymer catalyst can be attributed to not only to its Lewis acidity, but also to its hydrophilicity which improves the mass transfer. Recycling characteristics of Al-loaded functional lignin biopolymer Al_1-Lbp was confirmed with fructose yields remaining above 58 % after 8 cycles of use. The Al-loaded functional lignin biopolymer catalyst with its oxidized-lignin support is selective, recyclable and stable, making it a promising candidate for use in green and efficient processes for isomerization of glucose to fructose.

CRediT authorship contribution statement

Xinhua Qi: Writing – review & editing, Supervision, Methodology. **Richard Lee Smith Jr:** Writing – review & editing, Supervision, Software. **Haixin Guo:** Writing – review & editing, Writing – original draft, Project administration, Methodology, Investigation, Funding acquisition, Data curation, Conceptualization. **Jianrong Shan:** Writing – original draft, Investigation, Data curation. **Jirui Yang:** Writing – review & editing, Resources, Data curation. **Mo Qiu:** Writing – review & editing, Data curation. **Feng Shen:** Writing – review & editing, Software, Resources. **Jiajiang Zhou:** Writing – original draft, Software, Conceptualization.

Declaration of Competing Interest

The authors declare that they have no known competing financial interests or personal relationships that could have appeared to influence the work reported in this paper.

Data Availability

No data was used for the research described in the article.

Acknowledgments

The authors are grateful for Elite Youth program of the Chinese Academy of Agricultural Sciences (to Haixin Guo) and Key Laboratory of Technologies and Models for Cyclic Utilization from Agricultural Resources, Ministry of Agriculture and Rural Affairs, P. R. China (KLTMCUAR2023–02).

Appendix A. Supporting information

Supplementary data associated with this article can be found in the online version at doi:10.1016/j.apcatb.2024.124095.

References

[1] I. Khan, D. Tan, S.T. Hassan, Bilal, Role of alternative and nuclear energy in stimulating environmental sustainability: impact of government expenditures, Environ. Sci. Pollut. Res. 29 (2022) 37894–37905, https://doi.org/10.1007/s11356-021-18306-4.

[2] J. Liang, J. Chen, S. Wu, C. Liu, M. Lei, Comprehensive insights into cellulose structure evolution *via* multi-perspective analysis during a slow pyrolysis process, Sustain. Energy Fuels 2 (2018) 1855–1862, https://doi.org/10.1039/c8se00166a.

[3] Q. Hou, M.L.U. Rehman, X. Bai, C. Xie, R. Lai, H. Qian, T. Xia, G. Yu, Y. Tang, H. Xie, M. Ju, Incorporation of MgO into nitrogen-doped carbon to regulate adsorption for near-equilibrium isomerization of glucose into fructose in water, Appl. Catal. B 342 (2024) 123443, https://doi.org/10.1016/j.apcatb.2023.123443.

[4] W. Deng, Y. Feng, J. Fu, H. Guo, Y. Guo, B. Han, Z. Jiang, L. Kong, C. Li, H. Liu, P.T. T. Nguyen, P. Ren, F. Wang, S. Wang, Y. Wang, Y. Wang, S.S. Wong, K. Yan, N. Yan, X. Yang, Y. Zhang, Z. Zhang, X. Zeng, H. Zhou, Catalytic conversion of lignocellulosic biomass into chemicals and fuels, Green. Energy Environ. 8 (2023) 10–114, https://doi.org/10.1016/j.gee.2022.07.003.

[5] T. Liu, D. Liu, X. Zhao, Efficient conversion of glucose to 5-hydroxymethylfurfural by synergetic catalysis of enzymes and chemical catalysts towards potential large-scale continuous operation, Chem. Eng. J. 459 (2023) 141552, https://doi.org/10.1016/j.cej.2023.141552.

[6] B. Cai, J. Feng, D. Guo, S. Wang, T. Ma, T.L. Eberhardt, H. Pan, Highly efficient isomerization of glucose to fructose over a novel aluminum doped graphitic carbon nitride bifunctional catalyst, J. Clean. Prod. 346 (2022) 131144, https://doi.org/10.1016/j.jclepro.2022.131144.

[7] W. Liu, Y. Zhang, M. Sun, X. Zhao, S. Li, X. Chen, L. Zhong, L. Kong, Li-promoted C_3N_4 catalyst for efficient isomerization of glucose into fructose at 50 °C in water, Green. Energy Environ. 459 (2023) 141552, https://doi.org/10.1016/j.gee.2023.04.005.

[8] X. Ye, X. Shi, J. Li, B. Jin, J. Cheng, Z. Ren, H. Zhong, L. Chen, X. Liu, F. Jin, T. Wang, Fabrication of Mg-Al hydrotalcite/carbon nanotubes hybrid base catalysts for efficient production of fructose from glucose, Chem. Eng. J. 440 (2022) 135844, https://doi.org/10.1016/j.cej.2022.135844.

[9] J.-J. Liu, G.-C. Zhang, S. Kwak, E.J. Oh, E.J. Yun, K. Chomvong, J.H.D. Cate, Y.-S. Jin, Overcoming the thermodynamic equilibrium of an isomerization reaction through oxidoreductive reactions for biotransformation, Nat. Commun. 10 (2019) 1356, https://doi.org/10.1038/s41467-019-09288-6.

[10] Q. Guo, L. Ren, S.M. Alhassan, M. Tsapatsis, Glucose isomerization in dioxane/water with Sn-β catalyst: improved catalyst stability and use for HMF production, Chem. Commun. 55 (2019) 14942–14945, https://doi.org/10.1039/c9cc07842h.

[11] J.C. Vega-Vila, J.W. Harris, R. Gounder, Controlled insertion of tin atoms into zeolite framework vacancies and consequences for glucose isomerization catalysis, J. Catal. 344 (2016) 108–120, https://doi.org/10.1016/j.jcat.2016.09.011.

[12] J.B. Mensah, I. Delidovich, P.J.C. Hausoul, L. Weisgerber, W. Schrader, R. Palkovits, Mechanistic studies of the $Cu(OH)^+$-catalyzed isomerization of glucose into fructose in water, ChemSusChem 11 (2018) 2579–2586, https://doi.org/10.1002/cssc.201800483.

[13] S. Behera, S. Mohapatra, B.C. Behera, H. Thatoi, Recent updates on green synthesis of lignin nanoparticle and its potential applications in modern biotechnology, Crit. Rev. Biotechnol. (2023), https://doi.org/10.1080/07388551.2023.2229512.

[14] W. Pei, Y. Yusufu, Y. Zhan, X. Wang, J. Gan, L. Zheng, P. Wang, K. Zhang, C. Huang, Biosynthesizing lignin dehydrogenation polymer to fabricate hybrid hydrogel composite with hyaluronic acid for cartilage repair, Adv. Compos. Hybrid. Mater. 6 (2023) 180, https://doi.org/10.1007/s42114-023-00758-6.

[15] P. Jedrzejczak, M.N. Collins, T. Jesionowski, L. Klapiszewski, The role of lignin and lignin-based materials in sustainable construction-a comprehensive review, Int. J. Biol. Macromol. 187 (2021) 624–650, https://doi.org/10.1016/j.ijbiomac.2021.07.125.

[16] N.W. Dulie, B. Woldeyes, H.D. Demsash, Synthesis of lignin-carbohydrate complex-based catalyst from Eragrostis tef straw and its catalytic performance in xylose dehydration to furfural, Int. J. Biol. Macromol. 171 (2021) 10–16, https://doi.org/10.1016/j.ijbiomac.2020.12.213.

[17] M. Mennani, M. Kasbaji, A. Ait Benhamou, A. Boussetta, Z. Kassab, M. El Achaby, N. Grimi, A. Moubarik, The potential of lignin-functionalized metal catalysts - a systematic review, Renew. Sustain. Energy Rev. 189 (2024) 113936, https://doi.org/10.1016/j.rser.2023.113936.

[18] J. Liu, L. Yang, E. Shuang, C. Jin, C. Gong, K. Sheng, X. Zhang, Facile one-pot synthesis of functional hydrochar catalyst for biomass valorization, Fuel 315 (2022) 123172, https://doi.org/10.1016/j.fuel.2022.123172.

[19] S. Wang, D. Guo, R. Kang, J. Feng, H. Pan, Fabrication of lignin-derived mesoporous carbon/magnesium oxide composites for microwave-assisted isomerization of glucose in water, Int. J. Biol. Macromol. 232 (2023) 123341, https://doi.org/10.1016/j.ijbiomac.2023.123341.

[20] A. Mancera, V. Fierro, A. Pizzi, S. Dumarçay, P. Gérardin, J. Velásquez, G. Quintana, A. Celzard, Physicochemical characterisation of sugar cane bagasse lignin oxidized by hydrogen peroxide, Polym. Degrad. Stab. 95 (2010) 470–476, https://doi.org/10.1016/j.polymdegradstab.2010.01.012.

[21] Y. Wang, X. Liu, L. Meng, T. Liu, Q. Qi, X. Han, J. Ma, Promotion of catalytic performance of Pd/Al_2O_3 for o-xylene oxidation by morphological control, Chem. Eng. J. 472 (2023) 145013, https://doi.org/10.1016/j.cej.2023.145013.

[22] Y. Shi, P. Chen, J. Chen, D. Chen, H. Shu, H. Jiang, X. Luo, Hollow Prussian blue analogue/g-C_3N_4 nanobox for all-solid-state asymmetric supercapacitor, Chem. Eng. J. 404 (2021) 126284, https://doi.org/10.1016/j.cej.2020.126284.

[23] T. Chhabra, J. Rohilla, V. Krishnan, Nanoarchitectonics of phosphomolybdic acid supported on activated charcoal for selective conversion of furfuryl alcohol and levulinic acid to alkyl levulinates, Mol. Catal. 519 (2022) 112135, https://doi.org/10.1016/j.mcat.2022.112135.

[24] T. Dowaki, H. Guo, R.L. Smith Jr, Cascade conversion and kinetic modeling of glucose transformation into mixed-biofuels *via* lignin-derived Lewis-Bronsted acid biochars, Renew. Energy 217 (2023) 119204, https://doi.org/10.1016/j.renene.2023.119204.

[25] J. Liu, X. Zhang, L. Yang, U.A. Danhassan, S. Zhang, M. Yang, K. Sheng, X. Zhang, Glucose isomerization catalyzed by swollen cellulose derived aluminum-hydrochar, Sci. Total Environ. 777 (2021) 146037, https://doi.org/10.1016/j.scitotenv.2021.146037.

[26] J. Liu, M. Yang, C. Gong, S. Zhang, K. Sheng, X. Zhang, Insights into the glucose isomerization mechanism of Al-hydrochar catalyst probed by Al-oxide species transformation, J. Environ. Chem. Eng. 9 (2021) 106721, https://doi.org/10.1016/j.jece.2021.106721.
[27] T. Lee, J. Fu, V. Basile, J.S. Corsi, Z. Wang, E. Detsi, Activated alumina as value-added byproduct from the hydrolysis of hierarchical nanoporous aluminum with pure water to generate hydrogen fuel, Renew. Energy 155 (2020) 189–196, https://doi.org/10.1016/j.renene.2020.03.072.
[28] L.-J. Liu, Z.-M. Wang, S. Fu, Z.-B. Si, Z. Huang, T.-H. Liu, H.-Q. Yang, C.-W. Hu, Catalytic mechanism for the isomerization of glucose into fructose over an aluminium-MCM-41 framework, Catal. Sci. Technol. 11 (2021) 1537–1543, https://doi.org/10.1039/d0cy01984d.
[29] X. Yu, L. Peng, X. Gao, L. He, K. Chen, One-step fabrication of carbonaceous solid acid derived from lignosulfonate for the synthesis of biobased furan derivatives, RSC Adv. 8 (2018) 15762–15772, https://doi.org/10.1039/c8ra02056f.
[30] D. Kang, X. Yu, M. Ge, F. Xiao, H. Xu, Novel Al-doped carbon nanotubes with adsorption and coagulation promotion for organic pollutant removal, J. Environ. Sci. 54 (2017) 1–12, https://doi.org/10.1016/j.jes.2016.04.022.
[31] F. Guo, F. Xu, R. Cai, D. Li, Q. Xu, X. Yang, Z. Wu, Y. Wang, Q. He, L. Ao, J. Vymazal, Y. Chen, Enhancement of denitrification in biofilters by immobilized biochar under low-temperature stress, Bioresour. Technol. 347 (2022) 126664, https://doi.org/10.1016/j.biortech.2021.126664.
[32] K. Lotz, A. Wuetscher, H. Duedder, C.M. Berger, C. Russo, K. Mukherjee, G. Schwaab, M. Havenith, M. Muhler, Tuning the properties of iron-doped porous graphitic carbon synthesized by hydrothermal carbonization of cellulose and subsequent pyrolysis, ACS Omega 4 (2019) 4448–4460, https://doi.org/10.1021/acsomega.8b03369.
[33] K. Sheng, S. Zhang, J. Liu, S. E, C. Jin, Z. Xu, X. Zhang, Hydrothermal carbonization of cellulose and xylan into hydrochars and application on glucose isomerization, J. Clean. Prod. 237 (2019) 117831, https://doi.org/10.1016/j.jclepro.2019.117831.
[34] A. Maulidya, Y. Yulizar, T. Utari, D.O.B. Apriandanu, Gold nanoparticles supported on Al_2O_3 using Tabebuia aurea leaf extract and catalytic properties for methylene blue reduction, IOP Conf. Ser.: Mater. Sci. Eng. 763 (2020) 012049, https://doi.org/10.1088/1757-899X/763/1/012049.
[35] X. Yang, Y. Zhang, L. Zhou, B. Gao, T. Lu, Y. Su, J. Xu, Production of lactic acid derivatives from sugars over post-synthesized Sn-Beta zeolite promoted by WO_3, Food Chem. 289 (2019) 285–291, https://doi.org/10.1016/j.foodchem.2019.03.039.
[36] A. Rezayan, K. Wang, R. Nie, T. Lu, J. Wang, Y. Zhang, C.C. Xu, Synthesis of bifunctional tin-based silica-carbon catalysts, Sn/KIT-1/C, with tunable acid sites for the catalytic transformation of glucose into 5-hydroxymethylfurfural, Chem. Eng. J. 429 (2022) 132261, https://doi.org/10.1016/j.cej.2021.132261.
[37] Y. Yu, Z. Tang, W. Liu, J. Wang, Z. Chen, K. Shen, R. Wang, H. Liu, X. Huang, Y. Liu, Enhanced catalytic oxidation performance of K^+-modified Ti-MWW through selective breaking of interfacial hydrogen-bonding interactions of H_2O_2, Appl. Catal. A 587 (2019) 117270, https://doi.org/10.1016/j.apcata.2019.117270.
[38] L. Peng, C. Tao, H. Yang, J. Zhang, H. Liu, Mechanistic insights into the effect of the feed concentration on product formation during acid-catalyzed conversion of glucose in ethanol, Green. Chem. 24 (2022) 5219–5227, https://doi.org/10.1039/d2gc00300g.
[39] A. Rudawska, E. Jacniacka, Analysis for determining surface free energy uncertainty by the Owen–Wendt method, Int. J. Adhes. Adhes. 29 (2009) 451–457, https://doi.org/10.1016/j.ijadhadh.2008.09.008.
[40] W. Fan, C. Liu, C. Hu, X. Liu, X. Wang, J. Wu, Z. Yu, P. Cheng, T. Yang, Q. Liu, Y. Qi, Transition metal single atoms anchoring VTe_2 for efficient overall water splitting and oxygen reduction reactions: a first principles study, Appl. Surf. Sci. 635 (2023) 157611, https://doi.org/10.1016/j.apsusc.2023.157611.
[41] I.K.M. Yu, X. Xiong, D.C.W. Tsang, L. Wang, A.J. Hunt, H. Song, J. Shang, Y.S. Ok, C.S. Poon, Aluminium-biochar composites as sustainable heterogeneous catalysts for glucose isomerisation in a biorefinery, Green. Chem. 21 (2019) 1267–1281, https://doi.org/10.1039/c8gc02466a.
[42] S. Zhang, K. Sheng, Y. Liang, J. Liu, E. Shuang, X. Zhang, Green synthesis of aluminum-hydrochar for the selective isomerization of glucose to fructose, Sci. Total Environ. 727 (2020) 138743, https://doi.org/10.1016/j.scitotenv.2020.138743.
[43] P.P. Upare, A. Chamas, J.H. Lee, J.C. Kim, S.K. Kwak, Y.K. Hwang, D.W. Hwang, Highly efficient hydrotalcite/1-Butanol catalytic system for the production of the high-yield fructose crystal from glucose, ACS Catal. 10 (2020) 1388–1396, https://doi.org/10.1021/acscatal.9b01650.
[44] Y. Liu, Q. Lin, Q. Zhan, H. Zhang, R. Zhu, X. Wang, L. Li, J. Ren, Gamma-valerolactone-enabled control chemoselective conversion of glucose to 1,6-anhydroglucose over HZSM-5 zeolite, Appl. Catal. B 344 (2024) 123623, https://doi.org/10.1016/j.apcatb.2023.123623.
[45] A. Tampierr, C. Russo, R. Marotta, M. Constanti, S. Contreras, F. Medina, Microwave-assisted condensation of bio-based hydroxymethylfurfural and acetone over recyclable hydrotalcite-related materials, Appl. Catal. B 282 (2021) 119599, https://doi.org/10.1016/j.apcatb.2020.119599.
[46] L. Dong, J. Morales-Vidal, L. Mu, L. Li, N. Lopez, J. Perez-Ramirez, Z. Chen, Selective hydrogenolysis of 5-hydroxymethylfurfural to 5-methylfurfural over Au/TiO_2, Appl. Catal. B 335 (2023), https://doi.org/10.1016/j.apcatb.2023.122893.
[47] M. Yabushita, N. Shibayama, K. Nakajima, A. Fukuoka, Selective glucose-to-fructose isomerization in ethanol catalyzed by hydrotalcites, ACS Catal. 9 (2019) 2101–2109, https://doi.org/10.1021/acscatal.8b05145.
[48] S. Xu, T. He, J. Li, Z. Huang, C. Hu, Enantioselective synthesis of D-lactic acid via chemocatalysis using MgO: Experimental and molecular-based rationalization of the triose's reactivity and preliminary insights with raw biomass, Appl. Catal. B 292 (2021) 120145, https://doi.org/10.1016/j.apcatb.2021.120145.
[49] I.K.M. Yu, A. Hanif, D.C.W. Tsang, J. Shang, Z. Su, H. Song, Y.S. Ok, C.S. Poon, Tuneable functionalities in layered double hydroxide catalysts for thermochemical conversion of biomass-derived glucose to fructose, Chem. Eng. J. 383 (2020) 122914, https://doi.org/10.1016/j.cej.2019.122914.
[50] X. Ye, X. Shi, B. Jin, H. Zhong, F. Jin, T. Wang, Natural mineral bentonite as catalyst for efficient isomerization of biomass-derived glucose to fructose in water, Sci. Total Environ. 778 (2021) 146276, https://doi.org/10.1016/j.scitotenv.2021.146276.
[51] J. Tang, X. Guo, L. Zhu, C. Hu, Mechanistic study of glucose-to-fructose isomerization in water catalyzed by $Al(OH)_2(aq)^+$, ACS Catal. 5 (2015) 5097–5103, https://doi.org/10.1021/acscatal.5b01237.
[52] M. Culebras, M. Pishnamazi, G.M. Walker, M.N. Collins, Facile tailoring of structures for controlled release of paracetamol from sustainable lignin derived platforms, Molecules 26 (2021) 1593, https://doi.org/10.3390/molecules26061593.
[53] Y. Zhang, Z. Huang, R. Zhang, Facile fabrication of magnesium-enriched porous carbon for highly active and stable isomerization of glucose in water, J. Clean. Prod. 425 (2023) 138950, https://doi.org/10.1016/j.jclepro.2023.138950.
[54] N. Rajabbeigi, A.I. Torres, C.M. Lew, B. Elyassi, L. Ren, Z. Wang, H.J. Cho, W. Fan, P. Daoutidis, M. Tsapatsis, On the kinetics of the isomerization of glucose to fructose using Sn-Beta, Chem. Eng. J. 116 (2014) 235–242, https://doi.org/10.1016/j.ces.2014.04.031.
[55] R. Bermejo-Deval, R. Gounder, M.E. Davis, Framework and extraframework tin sites in zeolite beta react glucose differently, ACS Catal. 2 (2012) 2705–2713, https://doi.org/10.1021/cs300474x.
[56] T.R. Josephson, R.F. DeJaco, S. Pahari, L. Ren, Q. Guo, M. Tsapatsis, J.I. Siepmann, D.G. Vlachos, S. Caratzoulas, Cooperative catalysis by surface lewis acid/silanol for selective fructose etherification on Sn-SPP zeolite, ACS Catal. 8 (2018) 9056–9065, https://doi.org/10.1021/acscatal.8b01615.
[57] Y. Ma, H. Wang, Z. Wu, W. Tan, G. Feng, J. Jiang, A process insight into production of ethyl levulinate via a stepwise fractionation, J. Bioresour. Bioprod. 9 (2024) 233–242, https://doi.org/10.1016/j.jobab.2023.11.001.
[58] M.M. Zainol, M. Asmadi, N.A.S. Amin, M.N.F. Roslan, Glucose-derived bio-fuel additive via ethanolysis catalyzed by zinc modified sulfonated carbon, Int. Symp. React. Eng., Catal. Sustain. Energy (RECaSE) 57 (2021) 1008–1013, https://doi.org/10.1016/j.matpr.2021.08.065.